

# Residual 3D Scene Flow Learning with Context-Aware Feature Extraction\*

Guangming Wang, Yunzhe Hu, Xinrui Wu, and Hesheng Wang

**Abstract**—Scene flow estimation is the task to predict the point-wise 3D displacement vector between two consecutive frames of point clouds, which has important application in fields such as service robots and autonomous driving. Although many previous works have explored greatly on scene flow estimation based on point clouds, we point out two problems that have not been noticed or well solved before: 1) Points of adjacent frames in repetitive patterns may be wrongly associated due to similar spatial structure in their neighbourhoods; 2) Scene flow between adjacent frames of point clouds with long-distance movement may be inaccurately estimated. To solve the first problem, we propose a novel context-aware set conv layer to exploit contextual structure information of Euclidean space and learn soft aggregation weights for local point features. Our design is inspired by human perception of contextual structure information during scene understanding. We incorporate the context-aware set conv layer in a context-aware point feature pyramid module of 3D point clouds for scene flow estimation. For the second problem, we propose an explicit residual flow learning structure in the residual flow refinement layer to cope with long-distance movement. The experiments and ablation study on FlyingThings3D and KITTI scene flow datasets demonstrate the effectiveness of each proposed component and that we solve problem of ambiguous inter-frame association and long-distance movement estimation. Quantitative results on both FlyingThings3D and KITTI scene flow datasets show that our method achieves state-of-the-art performance, surpassing all other previous works to the best of our knowledge by at least 25%.

## I. INTRODUCTION

Scene flow represents a 3D vector field that comprises point-wise motion between two consecutive frames of point clouds. It provides a low-level and fundamental understanding of the motion of objects in a dynamic scene. Scene flow estimation can benefit many other fields such as robotics and autonomous driving. The low-level information of scene flow can also be extended to other tasks such as LiDAR odometry [1], point cloud registration [2], etc.

Traditional works [3], [4], [5] mainly focus on acquiring optical flow and disparity from stereo or RGB-D images and

\*This work was supported in part by the Natural Science Foundation of China under Grant 62073222 and U1913204, in part by “Shu Guang” project supported by Shanghai Municipal Education Commission and Shanghai Education Development Foundation under Grant 19SG08, in part by Shenzhen Science and Technology Program under Grant JSGG20201103094400002, in part by the Science and Technology Commission of Shanghai Municipality under Grant 21511101900, in part by grants from NVIDIA Corporation. Corresponding Author: Hesheng Wang. The first two authors contributed equally.

G. Wang, Y. Hu, X. Wu, and H. Wang are with Department of Automation, Key Laboratory of System Control and Information Processing of Ministry of Education, Key Laboratory of Marine Intelligent Equipment and System of Ministry of Education, Shanghai Engineering Research Center of Intelligent Control and Management, Shanghai Jiao Tong University, Shanghai 200240, China.

extend the optical flow estimation to scene flow estimation. However, the performance of these methods is limited due to indirect optimization in the 3D environment. With the advancement of deep learning to process raw point clouds [6], [7] and the application of LiDAR, recent studies [2], [8], [9], [10] focus on estimating scene flow with two consecutive frames of raw 3D point clouds as inputs. These methods predict scene flow using only 3D coordinates as inputs in an end-to-end fashion and do not require any prior knowledge of scene structure. FLoNet3D [2] integrates set conv layers based on PointNet++ [7] to downsample input point clouds and learn deep hierarchical features, then introduces a flow embedding layer to associate points from their geometric similarities and encode the motions. The extracted flow embedding features are to be propagated through the set upconv layers to generate scene flow. HPLFlowNet [8] proposes CorrBCLs to learn the correlation between two point clouds. However, due to the interpolation on permutohedral lattice, information of point clouds is inevitably lost therefore limiting the network performance. PointPWC-Net [9] utilizes a patch-to-patch method to enlarge the receptive field of points while associating point clouds in cost volume layer. It is the first network to explore coarse-to-fine fashion on 3D point clouds. However, PointPWC-Net only uses the relative coordinates to learn the weights of points for flow embedding. HALFlow [10] points out that correlation weights are not only decided by Euclidean space but by feature space. It thus proposes a novel double attentive embedding layer with two stages of attention in flow embedding.

However, all of the aforementioned scene flow estimation methods do not tackle to problem of recognizing repetitive patterns or well solve inaccurate long-distance motion estimation in a dynamic environment. For example, when estimating the motion of a multi-layer bookshelf, the points on the first layer of the shelf may be wrongly associated with those of the adjacent frame on the second layer because both layers share similar spatial structure information and are close in 3D space. In addition, for a fast-moving car, accurate scene flow predictions may not be made because the distance between two frames of point clouds is too long.

To tackle these two practical challenges, we propose a novel context-aware set conv layer and a residual flow learning structure for the learning of 3D scene flow. For the first challenge of recognizing repetitive patterns, the key is to diminish the mismatch among the points in repetitive patterns. We argue that if points on a specific layer of a bookshelf store the information of which layer they belong to, then they can match the correct points on the same

layer during the inter-frame association of two point clouds. Therefore, we propose a context-aware set conv layer to enhance the recognition of relative spatial position of points in repetitive patterns during feature extraction. For the second challenge of long-distance motion estimation, PointPWC-Net [9] introduces a coarse-to-fine scene flow estimation method. It estimates residual flow embedding features after obtaining coarse dense flow embedding features, then computes the overall flow embedding features. However, residual flow embedding features will bring about fuzziness in motion. We notice that scene flow can be directly added in 3D space, so we propose to explicitly learn the residual scene flow instead of flow embedding features. The learned residual flow will be directly added to the interpolated coarse dense flow and obtain a refined scene flow. The explicit estimation of residual scene flow will compensate directly for the long-distance motion estimation.

We conduct experiments on FlyingThings3D [11] and KITTI Scene Flow 2015 [12] datasets. Our model is trained and evaluated on FlyingThings3D [11] dataset with synthetic data. We also evaluate our model without fine-tuning on KITTI Scene Flow [12] dataset with real-world LiDAR scans to demonstrate its generalization ability. Ablation study is conducted as well to present the contribution of each proposed component. Our main contributions are as follows:

- A novel context-aware set conv layer is proposed to improve the recognition of repetitive patterns in 3D space. Contextual structure information in Euclidean space is exploited to learn the soft aggregation weights for the feature extraction of local points, which allows the extracted points to recognize their global position in a repetitive structure.
- An explicit residual flow learning structure is proposed to compensate for long-distance motion. The learned residual flow is directly added to the coarse scene flow, which helps correct the estimated scene flow and eliminates the ambiguity from residual flow embedding features.
- Effectiveness of the proposed context-aware set conv layer and residual flow learning structure is demonstrated by ablation study. Quantitative results show that our method outperforms all the prior works by at least 25% on FlyingThings3D and KITTI Scene Flow datasets. Visualization of certain objects with repetitive patterns and long-distance movement demonstrates that we effectively handle the challenges brought by these two situations.

The rest of our paper is as follows: Section II summarizes the related work to this paper. Section III elaborates our network architecture and the details about each component. Experiment details and results are in Section IV. Our conclusion is in Section V.

## II. RELATED WORK

### A. Deep Learning On 3D Data

With the proposal of the pioneering work PointNet [6] and PointNet++ [7], deep learning on raw point clouds has

gained more and more attention than voxels [13], [14], [15], [16] and multi-view [17], [18] based methods. PointNet [6] is the first network to process unstructured point sets and it utilizes shared Multi-Layer Perceptron (MLP) and max-pooling to learn the global features of point clouds. Follow-up work PointNet++ [7] introduces a hierarchical fashion to learn features by aggregating local point features from neighbourhood points. SPLATNet [19] maps input points to a high-dimensional permutohedral lattice and adopts Bilateral Convolution Layer (BCL) [20] to perform convolutions on sparse lattice and smoothly interpolate filtered signals back to input points.

Some other works focus on point feature aggregation. RandLA-Net [21] introduces attentive pooling to replace max-pooling used in [7] and effectively preserves useful local features from a wide neighbourhood. SOE-Net [22] designs a point orientation-encoding unit to integrate local information from eight orientations divided by eight octants. DH3D [23] leverages Flex Convolution (FlexConv) [24] and Squeeze-and-Excitation (SE) block [25] to avoid loss of structural information of local clusters induced by PointNet-based feature extraction.

### B. Point Cloud Based Scene Flow Estimation

With the application of advanced LiDAR in autonomous driving and service robots, raw data of point clouds are becoming more accessible. Since the pioneering work of PointNet [6], multiple deep learning methods have been utilized on raw point clouds for different tasks. The efficiency and robustness of directly processing point clouds being validated in PointNet [6] and PointNet++ [7], point cloud based scene flow estimation methods using deep learning have been progressively explored.

Liu *et al.* [2] propose FFlowNet3D to learn scene flow end-to-end based on PointNet++ [7]. FlowNet3D uses set conv layer following the architecture from [7] to extract local features. Then, it uses one flow embedding layer to encode the motion between point clouds. A learnable set upconv layer is introduced to decode the flow embedding features and propagate coarse scene flow to a finer level to obtain the overall scene flow. Gu *et al.* [8] introduce HPLFlowNet by leveraging Bilateral Convolutional Layers (BCL) and propose three novel layer designs: DownBCL, UpBCL, and CorrBCL. HPLFlowNet interpolates signals from input point clouds onto a permutohedral lattice [26] and conducts sparse convolution on the lattice for scene flow estimation. FLOT [27] introduces an optimal transport module inspired by graph matching to learn the correspondences between two frames of point clouds. Wu *et al.* [9] present PointPWC-Net, which follows a coarse-to-fine style for scene flow estimation. PointPWC-Net adopts the cost volume structure extensively used in optical flow estimation [28] but extends it to a patch-to-patch manner. It uses MLP to learn the weights in aggregating the costs from different patches in the point clouds from adjacent frames. To improve the performance of cost volume, Wang *et al.* [10] propose a novel double attentive flow embedding structure. It softly weighs the

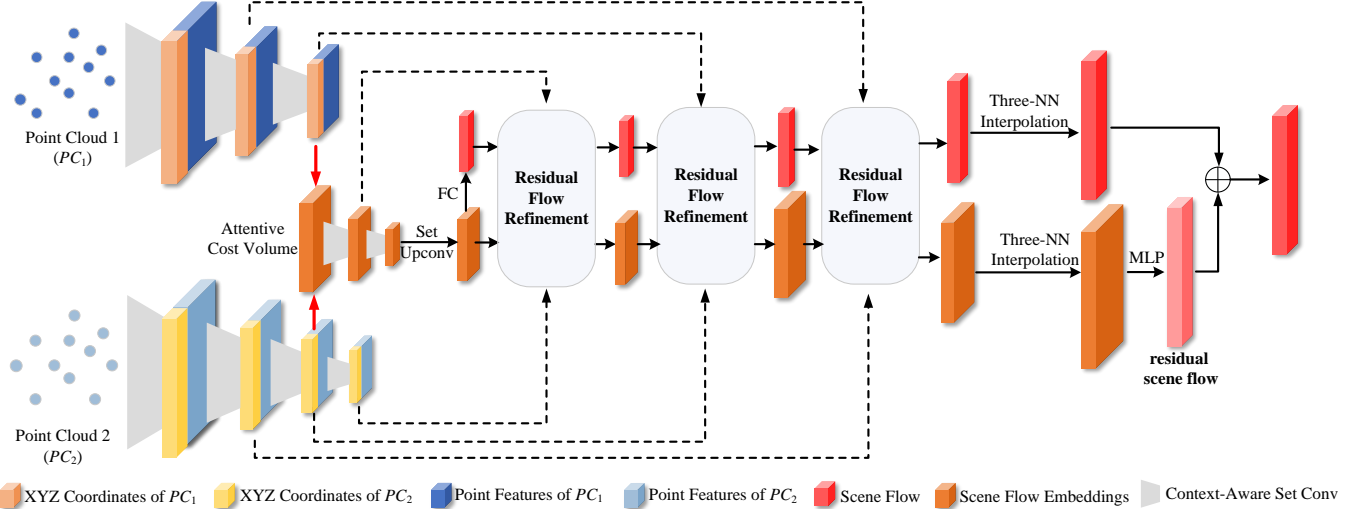


Fig. 1. The details of our network architecture. There are three proposed context-aware set conv layers for  $PC_1$  and four for  $PC_2$ . The same level of layers shares the same parameters. The attentive cost volume [10] is adopted to learn scene flow embedding features. Three proposed residual flow refinement layers are used in the flow refinement process. The scene flow between two point clouds are generated from coarse to fine.

neighbourhood point features to associate adjacent frames and allocates more attention on the regions with correct correspondences. [29] explores a weakly supervised learning algorithm by integrating flow into a high-level representation in the form of multi rigid-body motion. HCRF-Flow [30] combines the strengths of Deep Neural Networks (DNNs) and Conditional Random Fields (CRFs) to estimate scene flow and proposes a continuous high-order CRFs module to model the spatial smoothness and rigid motion constraints for the refinement of point-wise predictions. However, the above-mentioned methods do not well solve the problem of recognizing repetitive patterns or long-distance movements. Our paper focuses on solving these issues and proposes a novel context-aware set conv layer and residual flow learning structure to greatly improve the accuracy of scene flow estimation.

### III. CONTEXT-AWARE RESIDUAL FLOW LEARNING

#### A. Network Architecture

Our complete network architecture is illustrated in Fig. 1. Given two consecutive frames of point cloud scans, i.e.  $PC_1$  and  $PC_2$ , the proposed network predicts the 3D scene flow in a coarse-to-fine manner. Three main modules constitute our network: 1) Context-Aware Point Feature Pyramid, 2) Attentive Cost Volume, and 3) Hierarchical Residual Flow Refinement. The context-aware point feature pyramid module consists of three novel context-aware set conv layers for  $PC_1$  and four layers for  $PC_2$ , with each set conv layer applying downsampling operation and aggregating local point features attentively as shown in Fig. 2. The pyramid feature encoding structure for each point cloud shares the same weights. The same cost volume module is adopted from [10] followed by two set conv layers. Then, upsampled flow embedding features are obtained from the lowest level of flow embedding features by the set upconv

layer [2]. A coarse scene flow is first estimated by a simple shared Fully Connection (FC) layer on the upsampled flow embedding features. Next, the coarse scene flow and the upsampled flow embedding features are passed into three residual flow refinement layers to be refined iteratively and hierarchically. We last employ Three Nearest Neighbours (Three-NN) interpolation and MLP to attain the final residual scene flow and interpolated scene flow. The final estimated scene flow will be the summation of the final residual flow and the interpolated scene flow.

#### B. Context-Aware Point Feature Pyramid

In the context-aware point feature pyramid module, each point cloud is encoded through our novel context-aware set conv layer hierarchically. Unlike the set conv layer in [7] which simply uses MLP and max-pooling to extract local features for each point in the scene, our context-aware set conv layer employs the attention mechanism to avoid the point features lost in max-pooling operation.

In order to retain the features information of all the neighbouring points in the raw point sets, a means of weighted feature extraction from all neighbouring points is proposed. For the purpose of aggregating local point features and exploiting the contextual structure information in 3D Euclidean space, we adopt the information of coordinates and features to obtain weights for nearest neighbours of each sampled points. The whole process is shown in Fig. 2.

For each context-aware set conv layer, it takes  $n$  points  $\{p_i = \{x_i, p_{fi}\} \mid i = 1, \dots, n\}$  as input, where  $x_i \in \mathbb{R}^3$  denotes 3D coordinates and  $p_{fi} \in \mathbb{R}^c$  denotes local point features. The output is  $n'$  ( $n' < n$ ) sampled and encoded points  $\{p'_j = \{x'_j, p'_{fj}\} \mid j = 1, \dots, n'\}$ , where  $x'_j \in \mathbb{R}^3$  denotes 3D coordinates and  $p'_{fj} \in \mathbb{R}^{c'}$  denotes local point features. In the very first context-aware set conv layer of point feature pyramid,  $p_{fi}$  is equal to  $x_i$ . For  $n'$  output

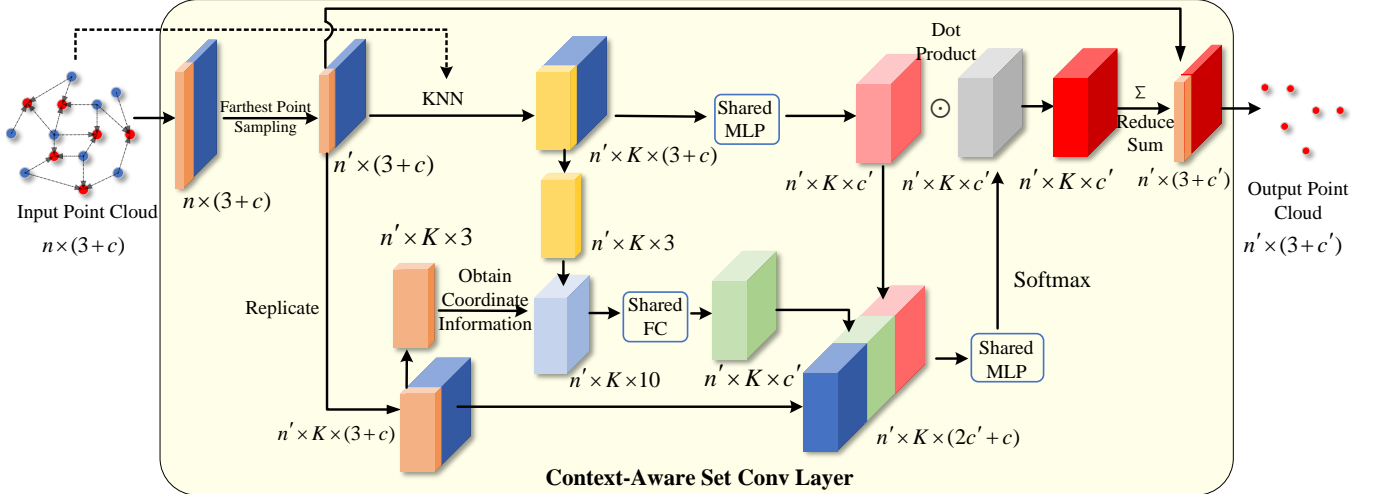


Fig. 2. The illustration of our novel context-aware set conv layer. Detailed process is elaborated in Section III-B.

points  $p'_j$ , the 3D coordinates  $x'_j$  are randomly sampled in the first layer and sampled by Farthest Point Sampling (FPS) algorithm in the subsequent layers, like [10]. The extraction process of point features  $pf'_j$  is elaborated as follows.

For each sampled point  $p'_j$ , its  $K$  nearest neighbours are searched and grouped from the unsampled  $n$  points as  $\{p_j^k = \{x_j^k, pf_j^k\} \mid k = 1, \dots, K\}$ . Then, a learnable shared MLP will be applied to extract the features  $pf_j'^k \in \mathbb{R}^c$  for the  $K$  neighbouring points  $p_j^k$  as follows:

$$pf_j'^k = \text{MLP}((x_j^k - x'_j) \oplus pf_j^k), \quad (1)$$

in which  $\oplus$  denotes concatenation operation of two vectors.

Instead of adopting max-pooling operation to aggregate local features for  $p'_j$ , we will exploit and leverage spatial structure information and feature information to regress soft aggregation weights. We first use  $x'_j$  and  $x_j^k$  to obtain 3D spatial structure information as follows:

$$d_j^k = x'_j \oplus x_j^k \oplus (x_j^k - x'_j) \oplus \|x_j^k - x'_j\|, \quad (2)$$

where  $\|\cdot\|$  indicates the  $L_2$  norm. The contextual aggregation weights are calculated as:

$$w_j^k = \text{softmax}(\text{MLP}(\text{FC}(d_j^k) \oplus pf_j'^k \oplus pf_j^k)). \quad (3)$$

In the calculation of contextual aggregation weights, the information of coordinates and relative position in 3D space of central point and its neighbours together with their features are utilized, which aims to encode the global position of central point in repetitive patterns.

Finally, the contextual aggregation weights are used to softly aggregate the neighbouring features for  $p'_j$ :

$$pf_j' = \sum_{k=1}^K pf_j'^k \odot w_j^k, \quad (4)$$

where  $\odot$  indicates dot product.

### C. Attentive Cost Volume

In order to learn the underlying motion information between two sets of points, we directly adopt the cost volume with attention in [10] to associate two point clouds. The attentive cost volume module produces flow embedding features from the output of the context-aware point feature pyramid module for the flow estimation and refinement in the later process.

For point cloud  $PC_1 = \{(x_i, f_i) \mid x_i \in \mathbb{R}^3, f_i \in \mathbb{R}^c, i = 1, \dots, n_1\}$  and point cloud  $PC_2 = \{(y_j, g_j) \mid y_j \in \mathbb{R}^3, g_j \in \mathbb{R}^c, i = 1, \dots, n_2\}$ , the flow embedding features  $E = \{(x_i, e_i) \mid x_i \in \mathbb{R}^3, e_i \in \mathbb{R}^{c'}, i = 1, \dots, n_1\}$  between two point clouds are learned from attentive cost volume.

### D. Hierarchical Residual Flow Refinement

The hierarchical residual flow refinement module mainly contains three residual flow refinement layers. The details of residual flow refinement layers are illustrated in Fig. 3. It contains four major components: 1) Set Upconv Layer, 2) Coordinates Warping Layers, 3) Attentive Cost Volume Layer, and 4) Scene Flow Predictor.

1) *Set Upconv Layer*: We adopt set upconv layer in [2] here to upsample coarse sparse flow embedding features. The inputs are  $n$  sparse points with sparse flow embedding features  $\{(x_i, e_i) \mid i = 1, \dots, n\}$  and  $n'$  ( $n' > n$ ) dense points  $\{(x'_j, pf'_j) \mid j = 1, \dots, n'\}$  from the previous context-aware set conv layer. The outputs will be  $n'$  dense flow embedding features  $\{(x'_j, e'_j) \mid j = 1, \dots, n'\}$ . To be specific, each of the dense points will search and select its  $K$  nearest neighbours in the sparse point sets, and the sparse flow embedding features will be aggregated into the dense flow embedding features in a learnable manner by shared MLP.

2) *Coordinates Warping Layer*: As a coarse-to-fine manner to refine scene flow, the input coarse sparse flow in Fig. 3 is first interpolated by Three-NN to obtain a coarse dense flow  $\{sf_i^{\text{dense}} \mid i = 1, \dots, n_1\}$ . Then  $PC_1 = \{(x_i, pf_i) \mid i = 1, \dots, n_1\}$  are warped by coarse dense flow to update the

coordinates. The warped point clouds are denoted as  $PC'_1 = \{(x'_i, pf_i) | i = 1, \dots, n_1\}$  where  $x'_i = x_i + sf_i^{dense}$ .

3) *Attentive Cost Volume Layer*: By taking in the warped point cloud  $PC'_1$  in Section III-D.2 and the second frame of point cloud  $PC_2$ , the same layer of attentive cost volume described in Section III-B is adopted here to compute new flow embedding features  $\{re_i | i = 1, \dots, n_1\}$ . “Attentive flow re-embedding features” is used in Fig. 3 to emphasize its significance for scene flow predictor.

The skip connection in Fig. 1 shows where  $PC_1$  and  $PC_2$  for each refinement layer come from.

4) *Scene Flow Predictor*: The scene flow predictor is designed to refine the coarse dense flow embedding features. There are three inputs to this layer: point features of  $PC_1 \{pf_i \in \mathbb{R}^{c_1} | i = 1, \dots, n_1\}$ , attentive flow re-embedding features  $\{re_i \in \mathbb{R}^{c_2} | i = 1, \dots, n_1\}$  generated in Section III-D.3, and the upsampled coarse dense flow embedding features  $\{e_i \in \mathbb{R}^{c_3} | i = 1, \dots, n_1\}$  from Section III-D.1. The refined scene flow embedding features are calculated as:

$$e'_i = MLP(pf_i \oplus re_i \oplus e_i). \quad (5)$$

Instead of directly generating the refined scene flow by applying shared FC to the refined flow embedding features in [10], we exploit an explicit residual flow estimation structure. The residual scene flow  $sf_i^{res}$  is first predicted by shared FC (implemented by  $1 \times 1$  convolution) on the refined scene flow embedding features. Then, the coarse dense flow  $sf_i^{dense}$  is added by the residual scene flow  $sf_i^{res}$  to generate the refined scene flow  $\{sf_i | i = 1, \dots, n_1\}$ :

$$sf_i^{res} = FC(e'_i), \quad (6)$$

$$sf_i = sf_i^{res} + sf_i^{dense}. \quad (7)$$

As shown in Fig. 1, the scene flow between two consecutive frames and scene flow embedding features are both refined through three residual flow refinement layers from coarse to fine. For the scene flow estimation of the finest level, we do not apply the residual flow refinement layer in order to save computational resources. Instead, we only use Three-NN interpolation and MLP to acquire the final residual scene flow and the overall scene flow.

Interpolation using three nearest neighbours from the preceding sparse layer is adopted to realize upsampling operation on flow embedding features while saving GPU memory. Then, MLP is used to predict final residual scene flow. Finally, the final residual scene flow is simply added to the interpolated coarse dense scene flow to obtain the overall 3D scene flow.

## IV. EXPERIMENTS

### A. Datasets and Data Preprocessing

We follow the supervised learning for scene flow estimation in our experiments. We first use the synthetic FlyingThings3D dataset [11] for both training and evaluation. Then, we also evaluate our trained model on real-world 3D scans from KITTI scene flow dataset [12] without fine-tuning to demonstrate its generalization ability.

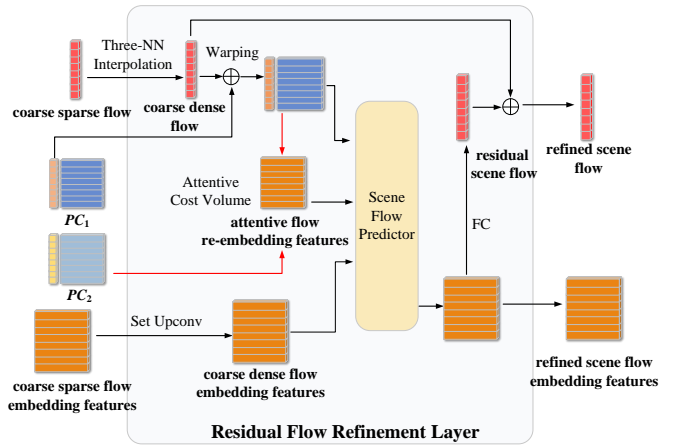


Fig. 3. The details of residual flow refinement layer in Section III-D.

Since the ground truth scene flow of large-scale real-world is difficult to acquire, we turn to the synthetic FlyingThings3D dataset [11] for our training. Following the preprocessing methods in [8], [9], [10], [29], [30], training and evaluation set are built by reconstructing ground truth scene flow and 3D point clouds from ground truth disparity map and optical flow. There are 19,640 pairs in training set and 3,824 pairs in the evaluation set. The points with depth larger than 35m are excluded.

KITTI Scene Flow 2015 dataset [12] is another widely used dataset for scene flow estimation. It comprises 200 scenes for training and 200 scenes for testing. To evaluate our model and conduct a fair comparative experiment with other previous works, we recover the ground truth scene flow and point clouds following procedures in [8], [9], [10], [29], [30]. Like FlyingThings3D [11], points with depth larger than 35m are also removed. The points from the ground with height less than 0.3m are also removed since they are of no significance for flow estimation. 142 scenes from the training set with raw 3D point clouds are used for evaluation since ground truth scene flow is not available in the test set.

### B. Training Details

1) *Training Loss*: We train our network with a multi-scale supervision style, like [28], [9]. Assume the ground truth scene flow at  $l$  level is  $SF^l = \{sf_i^l \in \mathbb{R}^3 | i = 1, \dots, N_l\}$ . The estimated scene flow at  $l$  level is  $SF^l = \{sf_i^l \in \mathbb{R}^3 | i = 1, \dots, N_l\}$ .  $N_l$  denotes the number of points at  $l$  level. Then multi-scale loss is formulated as:

$$Loss = \sum_{l=1}^4 \phi_l \frac{1}{N_l} \sum_{i=1}^{N_l} \left\| sf_i^l - sf_i^l \right\|_2, \quad (8)$$

where  $\|\cdot\|_2$  denotes  $L_2$  norm and  $\phi_l$  is the weight of loss at  $l$  level. We consider the last and finest scene flow as the  $l = 1$  level flow. In our network, the input point clouds have  $4N = 8192$  points and  $N_1 = N = 2048$ ,  $N_2 = N/2 = 1024$ ,  $N_3 = N/8 = 256$ , and  $N_4 = N/32 = 64$ . The weights are set as  $\phi_1 = 0.2$ ,  $\phi_2 = 0.4$ ,  $\phi_3 = 0.8$ , and  $\phi_4 = 1.6$ .

TABLE I

COMPARISON RESULTS BETWEEN RECENT METHODS AND OURS ON FLYINGTHINGS3D [11] AND KITTI SCENE FLOW [12] DATASETS. ALL LISTED APPROACHES ARE ONLY TRAINED ON FLYINGTHINGS3D DATASET [11]. KITTI SCENE FLOW [12] DATASET IS USED TO TEST THE GENERALIZATION ABILITY OF MODELS. THE BEST RESULTS ARE HIGHLIGHTED IN BOLD.

Evaluation Dataset	Method	Training Data	Input	EPE3D	Acc3D Strict	Acc3D Relax	Outliers3D	EPE2D	Acc2D
FlyingThings 3D dataset [11]	FlowNet3 [31]	Quarter	RGB stereo	0.4570	0.4179	0.6168	0.6050	5.1348	0.8125
	ICP [32]	No	Points	0.4062	0.1614	0.3038	0.8796	23.2280	0.2913
	FlowNet3D [2]	Quarter	Points	0.1136	0.4125	0.7706	0.6016	5.9740	0.5692
	SPLATFlowNet [19]	Quarter	Points	0.1205	0.4197	0.7180	0.6187	6.9759	0.5512
	HPLFlowNet [8]	Quarter	Points	0.0804	0.6144	0.8555	0.4287	4.6723	0.6764
	HPLFlowNet [8]	Complete	Points	0.0696	—	—	—	—	—
	PointPWC-Net [9]	Complete	Points	0.0588	0.7379	0.9276	0.3424	3.2390	0.7994
	HALFlow [10]	Quarter	Points	0.0511	0.7808	0.9437	0.3093	2.8739	0.8056
	HALFlow [10]	Complete	Points	0.0492	0.7850	0.9468	0.3083	2.7555	0.8111
	FLOT [27]	Complete	Points	0.0520	0.7320	0.9270	0.3570	—	—
	Rigid3DSceenFlow [29]	Complete	Points	0.0520	0.7460	0.9360	0.3610	—	—
	HCRF-Flow [30]	Quarter	Points	0.0488	0.8337	0.9507	0.2614	2.5652	0.8704
KITTI dataset [12]	Ours	Quarter	Points	0.0360	0.8894	0.9680	0.1827	2.0418	0.8888
	Ours	Complete	Points	<b>0.0310</b>	<b>0.9139</b>	<b>0.9768</b>	<b>0.1551</b>	<b>1.7504</b>	<b>0.9113</b>
	FlowNet3 [31]	Quarter	RGB stereo	0.9111	0.2039	0.3587	0.7463	5.1023	0.7803
	ICP [32]	No	Points	0.5181	0.0669	0.1667	0.8712	27.6752	0.1056
KITTI dataset [12]	FlowNet3D [2]	Quarter	Points	0.1767	0.3738	0.6677	0.5271	7.2141	0.5093
	SPLATFlowNet [19]	Quarter	Points	0.1988	0.2174	0.5391	0.6575	8.2306	0.4189
	HPLFlowNet [8]	Quarter	Points	0.1169	0.4783	0.7776	0.4103	4.8055	0.5938
	HPLFlowNet [8]	Complete	Points	0.1113	—	—	—	—	—
	PointPWC-Net [9]	Complete	Points	0.0694	0.7281	0.8884	0.2648	3.0062	0.7673
	HALFlow [10]	Quarter	Points	0.0692	0.7532	0.8943	0.2529	2.8660	0.7811
	HALFlow [10]	Complete	Points	0.0622	0.7649	0.9026	0.2492	2.5140	0.8128
	FLOT [27]	Complete	Points	0.0560	0.7550	0.9080	0.2420	—	—
	Rigid3DSceenFlow [29]	Complete	Points	0.0420	0.8490	0.9590	0.2080	—	—
	HCRF-Flow [30]	Quarter	Points	0.0531	0.8631	0.9444	0.1797	2.0700	0.8656
	Ours	Quarter	Points	0.0396	0.8679	0.9526	0.1722	1.5517	0.9125
	Ours	Complete	Points	<b>0.0351</b>	<b>0.8932</b>	<b>0.9620</b>	<b>0.1654</b>	<b>1.2879</b>	<b>0.9442</b>

TABLE II  
ABLATION STUDY ON CONTEXT-AWARE SET CONV LAYER AND RESIDUAL FLOW LEARNING.

Dataset	Method	EPE3D	Acc3D Strict	Acc3D Relax	Outliers	EPE2D	Acc2D
FlyingThings 3D dataset [11]	Baseline	0.0607	0.6977	0.9349	0.3366	3.3218	0.7591
	Baseline + Context-aware set conv layer	0.0559	0.7481	0.9468	0.3024	3.0917	0.7964
	Baseline + Residual flow learning	0.0384	0.8757	0.9637	0.1996	2.1914	0.8765
	Ours (Baseline + Context-aware set conv layer + Residual flow learning)	<b>0.0360</b>	<b>0.8894</b>	<b>0.9680</b>	<b>0.1827</b>	<b>2.0418</b>	<b>0.8888</b>

2) *Implementation Details*: During the training and evaluation of our network, two consecutive frames of point clouds are randomly sampled to generate 8192 points as inputs, respectively. Following [2], [8], [9], [10], [30], the input point clouds of our network only contains 3D XYZ coordinates.  $\frac{1}{4}$  of the training set (4910 pairs) of FlyingThings3D [11] dataset is first used to train our model and then complete training set is used to fine-tune our model in order to facilitate the training process. We conduct all the experiments on a single Titan RTX GPU with PyTorch 1.5.0. Adam optimizer [33] is adopted in the training process with  $\beta_1 = 0.9$  and  $\beta_2 = 0.99$ . The learning rate is initialized with 0.001 and exponentially decays with decay rate  $\gamma = 0.5$ . The step size for decaying is 80. The batchsize is set as 20.

### C. Evaluation Metrics

The same evaluation metrics as [2], [8], [9], [10], [30] are adopted to evaluate our model for a fair comparison with

other methods. Let  $sf_i$  be the ground truth scene flow and  $\bar{sf}_i$  be the overall predicted scene flow.

$$\text{EPE3D}(m): \frac{1}{N} \sum_{i=1}^N \|\bar{sf}_i - sf_i\|_2.$$

**Acc3D Strict**: Percentage of  $\bar{sf}_i$  such that  $\|\bar{sf}_i - sf_i\|_2 < 0.05m$  or  $\frac{\|\bar{sf}_i - sf_i\|_2}{\|sf_i\|_2} < 5\%$ .

**Acc3D Relax**: Percentage of  $\bar{sf}_i$  such that  $\|\bar{sf}_i - sf_i\|_2 < 0.1m$  or  $\frac{\|\bar{sf}_i - sf_i\|_2}{\|sf_i\|_2} < 10\%$ .

**Outliers3D**: Percentage of  $\bar{sf}_i$  such that  $\|\bar{sf}_i - sf_i\|_2 > 0.3m$  or  $\frac{\|\bar{sf}_i - sf_i\|_2}{\|sf_i\|_2} > 10\%$ .

**EPE2D**:  $\frac{1}{N} \sum_{i=1}^N \|\bar{of}_i - of_i\|_2$ , where  $of_i$  stands for the ground truth optical flow and  $\bar{of}_i$  stands for the predicted optical flow from the projections of input point clouds and the point clouds synthesized by predicted 3D scene flow.

**Acc2D**: Percentage of  $\bar{of}_i$  such that  $\|\bar{of}_i - of_i\|_2 < 3px$  or  $\frac{\|\bar{of}_i - of_i\|_2}{\|of_i\|_2} < 5\%$ .

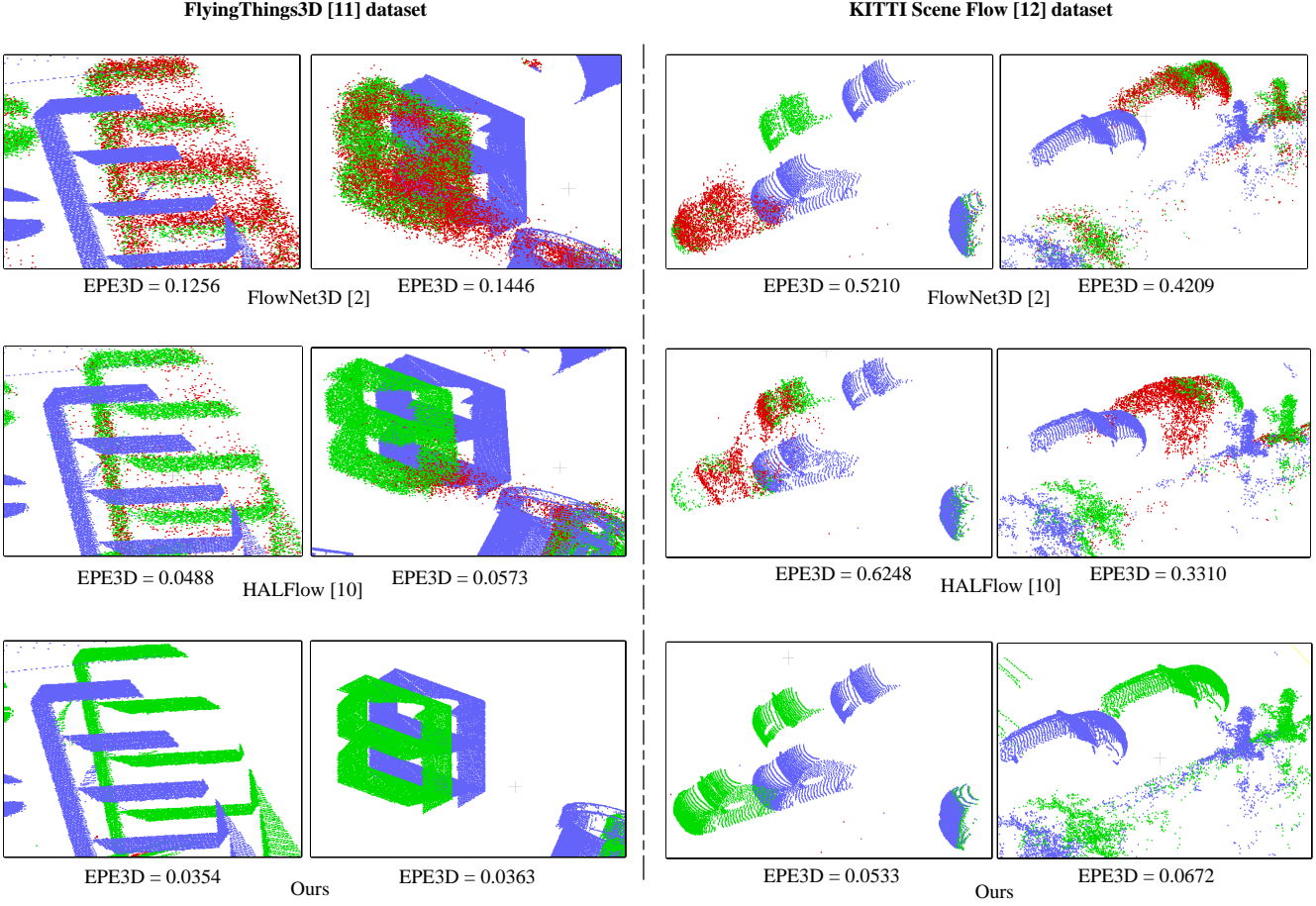


Fig. 4. Detailed visualization comparison among FlowNet3D [2], HALFflow [10], and our method for scene flow estimation. Blue points are  $PC_1$ . Green points represent accurate predictions  $PC_2 = PC_1 + SF$  and red points represent inaccurate predictions (Accuracy is measured by Acc3D Relax).

#### D. Results

1) *Comparison With State-of-the-Art (SOTA)*: Our method outperforms all other methods as quantitative evaluation results shown in Table I. It can be seen that our method surpasses SOTA method HCRF-Flow [30] by 26% on EPE3D on FlyingThings3D dataset, and achieves the best results on all 3D and 2D metrics. Our method also outperforms all other previous works remarkably on KITTI scene flow dataset [12], which strongly demonstrated the generalization ability of our method on real-world 3D data. Noticeably, recent SOTA methods [29], [30] impose rigid-body motion constraints while ours does not and outperforms them by a large margin.

Qualitative results in Fig. 4 shows detailed visualization of the accuracy of the predicted scene flow by our method and other methods [2], [10]. For a structure with repetitive patterns like the multi-layer bookshelf shown in Fig. 4, points are likely to be estimated with inaccurate scene flow for FlowNet3D [2] and HALFflow [10]. We believe that points of  $PC_1$  on a certain layer of the shelf learn the wrong correspondence with  $PC_2$  due to similar and repetitive 3D structure. By comparison, our method introduces context-aware set conv layer during feature extraction and performs better on repetitive patterns. The context-aware set conv

layer utilizes 3D coordinates information and relative position information from neighbourhood points together with feature information to extract context-aware point features. It allows the extracted local features to encode the correct global position within repetitive patterns in Euclidean space, providing more distinguishable positional cue for learning the right correspondence in the subsequent operation. For the scenes with long-distance motion on the right in Fig. 4, our method performs the best among the three methods. We believe that it is the residual flow learning structure that contributes to the precise flow estimation. Explicit estimation of residual flow allows the coarse scene flow to be corrected with clear direction and compensates the errors successively by residual flow refinement layers.

2) *Ablation Study*: In this paper, a novel context-aware set conv layer and residual flow learning structure are proposed. In order to validate the effectiveness of each component, our network is trained and evaluated without either or both of the components using one quarter of the training set (4910 pairs). Other experiment settings are the same as Section IV-D.1. In Table II, the method without context-aware set conv layer means removing the contextual weighting structure. Experiment results in Table II show that both of our proposed components improve the performance greatly.

## V. CONCLUSION

In this paper, a novel context-aware feature encoding layer and a residual flow learning structure are proposed. Inspired by human attention on contextual perception and relocation by recognizing repetitive structure in space, our proposed context-aware set conv layer aggregates point features utilizing 3D spatial structure and feature information for soft aggregation. Explicit residual flow learning is proposed to contribute to precise long-distance motion learning. Ablation study is conducted to demonstrate their effectiveness for scene flow estimation.

Experiments on FlyingThings3D [11] and KITTI scene flow datasets [12] shows that our method achieves state-of-the-art performance. We believe this context-aware feature extraction method and residual flow structure can improve the perception of repetitive patterns and long-distance motion estimation between two point clouds, which will provide some enlightenment for tasks with inter-frame association like registration, motion estimation, etc.

## REFERENCES

- [1] G. Wang, X. Wu, Z. Liu, and H. Wang, “Pwclo-net: Deep lidar odometry in 3d point clouds using hierarchical embedding mask optimization,” in *Proceedings of the IEEE/CVF Conference on Computer Vision and Pattern Recognition*, 2021, pp. 15910–15919.
- [2] X. Liu, C. R. Qi, and L. J. Guibas, “Flownet3d: Learning scene flow in 3d point clouds,” in *Proceedings of the IEEE/CVF Conference on Computer Vision and Pattern Recognition*, 2019, pp. 529–537.
- [3] C. Vogel, K. Schindler, and S. Roth, “3d scene flow estimation with a piecewise rigid scene model,” *International Journal of Computer Vision*, vol. 115, no. 1, pp. 1–28, 2015.
- [4] M. Menze and A. Geiger, “Object scene flow for autonomous vehicles,” in *Proceedings of the IEEE conference on computer vision and pattern recognition*, 2015, pp. 3061–3070.
- [5] A. Wedel, T. Brox, T. Vaudrey, C. Rabe, U. Franke, and D. Cremers, “Stereoscopic scene flow computation for 3d motion understanding,” *International Journal of Computer Vision*, vol. 95, no. 1, pp. 29–51, 2011.
- [6] C. R. Qi, H. Su, K. Mo, and L. J. Guibas, “Pointnet: Deep learning on point sets for 3d classification and segmentation,” in *Proceedings of the IEEE Conference on Computer Vision and Pattern Recognition*, 2017, pp. 652–660.
- [7] C. R. Qi, L. Yi, H. Su, and L. J. Guibas, “Pointnet++: Deep hierarchical feature learning on point sets in a metric space,” *arXiv preprint arXiv:1706.02413*, 2017.
- [8] X. Gu, Y. Wang, C. Wu, Y. J. Lee, and P. Wang, “Hplflownet: Hierarchical permutohedral lattice flownet for scene flow estimation on large-scale point clouds,” in *Proceedings of the IEEE Conference on Computer Vision and Pattern Recognition*, 2019, pp. 3254–3263.
- [9] W. Wu, Z. Y. Wang, Z. Li, W. Liu, and L. Fuxin, “Pointpwc-net: Cost volume on point clouds for (self-) supervised scene flow estimation,” in *European Conference on Computer Vision*. Springer, 2020, pp. 88–107.
- [10] G. Wang, X. Wu, Z. Liu, and H. Wang, “Hierarchical attention learning of scene flow in 3d point clouds,” *IEEE Transactions on Image Processing*, vol. 30, pp. 5168–5181, 2021.
- [11] N. Mayer, E. Ilg, P. Hausser, P. Fischer, D. Cremers, A. Dosovitskiy, and T. Brox, “A large dataset to train convolutional networks for disparity, optical flow, and scene flow estimation,” in *Proceedings of the IEEE conference on computer vision and pattern recognition*, 2016, pp. 4040–4048.
- [12] M. Menze, C. Heipke, and A. Geiger, “Object scene flow,” *ISPRS Journal of Photogrammetry and Remote Sensing*, vol. 140, pp. 60–76, 2018.
- [13] Z. Wu, S. Song, A. Khosla, F. Yu, L. Zhang, X. Tang, and J. Xiao, “3d shapenets: A deep representation for volumetric shapes,” in *Proceedings of the IEEE conference on computer vision and pattern recognition*, 2015, pp. 1912–1920.
- [14] D. Maturana and S. Scherer, “Voxnet: A 3d convolutional neural network for real-time object recognition,” in *2015 IEEE/RSJ International Conference on Intelligent Robots and Systems (IROS)*. IEEE, 2015, pp. 922–928.
- [15] G. Riegler, A. Osman Ulusoy, and A. Geiger, “Octnet: Learning deep 3d representations at high resolutions,” in *Proceedings of the IEEE conference on computer vision and pattern recognition*, 2017, pp. 3577–3586.
- [16] D. C. Garcia, T. A. Fonseca, R. U. Ferreira, and R. L. de Queiroz, “Geometry coding for dynamic voxelized point clouds using octrees and multiple contexts,” *IEEE Transactions on Image Processing*, vol. 29, pp. 313–322, 2019.
- [17] H. Su, S. Maji, E. Kalogerakis, and E. Learned-Miller, “Multi-view convolutional neural networks for 3d shape recognition,” in *Proceedings of the IEEE international conference on computer vision*, 2015, pp. 945–953.
- [18] E. Kalogerakis, M. Averkiou, S. Maji, and S. Chaudhuri, “3d shape segmentation with projective convolutional networks,” in *proceedings of the IEEE conference on computer vision and pattern recognition*, 2017, pp. 3779–3788.
- [19] H. Su, V. Jampani, D. Sun, S. Maji, E. Kalogerakis, M.-H. Yang, and J. Kautz, “Splatnet: Sparse lattice networks for point cloud processing,” in *Proceedings of the IEEE conference on computer vision and pattern recognition*, 2018, pp. 2530–2539.
- [20] V. Jampani, M. Kiefel, and P. V. Gehler, “Learning sparse high dimensional filters: Image filtering, dense crfs and bilateral neural networks,” in *Proceedings of the IEEE Conference on Computer Vision and Pattern Recognition*, 2016, pp. 4452–4461.
- [21] Q. Hu, B. Yang, L. Xie, S. Rosa, Y. Guo, Z. Wang, N. Trigoni, and A. Markham, “Randla-net: Efficient semantic segmentation of large-scale point clouds,” in *Proceedings of the IEEE/CVF Conference on Computer Vision and Pattern Recognition*, 2020, pp. 11108–11117.
- [22] Y. Xia, Y. Xu, S. Li, R. Wang, J. Du, D. Cremers, and U. Stilla, “Soenet: A self-attention and orientation encoding network for point cloud based place recognition,” in *Proceedings of the IEEE/CVF Conference on Computer Vision and Pattern Recognition*, 2021, pp. 11348–11357.
- [23] J. Du, R. Wang, and D. Cremers, “Dh3d: Deep hierarchical 3d descriptors for robust large-scale 6dof relocation,” in *European Conference on Computer Vision*. Springer, 2020, pp. 744–762.
- [24] F. Groh, P. Wieschollek, and H. P. Lensch, “Flex-convolution,” in *Asian Conference on Computer Vision*. Springer, 2018, pp. 105–122.
- [25] J. Hu, L. Shen, and G. Sun, “Squeeze-and-excitation networks,” in *Proceedings of the IEEE conference on computer vision and pattern recognition*, 2018, pp. 7132–7141.
- [26] A. Adams, J. Baek, and M. A. Davis, “Fast high-dimensional filtering using the permutohedral lattice,” in *Computer graphics forum*, vol. 29, no. 2. Wiley Online Library, 2010, pp. 753–762.
- [27] G. Puy, A. Boulch, and R. Marlet, “Flot: Scene flow on point clouds guided by optimal transport,” in *Computer Vision–ECCV 2020: 16th European Conference, Glasgow, UK, August 23–28, 2020, Proceedings, Part XXVIII 16*. Springer, 2020, pp. 527–544.
- [28] D. Sun, X. Yang, M.-Y. Liu, and J. Kautz, “Pwc-net: Cnns for optical flow using pyramid, warping, and cost volume,” in *Proceedings of the IEEE conference on computer vision and pattern recognition*, 2018, pp. 8934–8943.
- [29] Z. Gojcic, O. Litany, A. Wieser, L. J. Guibas, and T. Birdal, “Weakly supervised learning of rigid 3d scene flow,” in *Proceedings of the IEEE/CVF Conference on Computer Vision and Pattern Recognition*, 2021, pp. 5692–5703.
- [30] R. Li, G. Lin, T. He, F. Liu, and C. Shen, “Hcrf-flow: Scene flow from point clouds with continuous high-order crfs and position-aware flow embedding,” in *Proceedings of the IEEE/CVF Conference on Computer Vision and Pattern Recognition*, 2021, pp. 364–373.
- [31] E. Ilg, T. Saikia, M. Keuper, and T. Brox, “Occlusions, motion and depth boundaries with a generic network for disparity, optical flow or scene flow estimation,” in *Proceedings of the European Conference on Computer Vision (ECCV)*, 2018, pp. 614–630.
- [32] P. J. Besl and N. D. McKay, “Method for registration of 3-d shapes,” in *Sensor fusion IV: control paradigms and data structures*, vol. 1611. International Society for Optics and Photonics, 1992, pp. 586–606.
- [33] D. P. Kingma and J. Ba, “Adam: A method for stochastic optimization,” *arXiv preprint arXiv:1412.6980*, 2014.